Chromium (III), Titanium (III), and Vanadium (IV) Sensitization of Rare Earth Complexes for Luminescent Solar Concentrator Applications

by

Nicholas John Thompson

Submitted to the Department of Materials Science and Engineering
in partial fulfillment of the requirements for the degree of

Master of Science in Materials Science and Engineering

at the

MASSACHUSETTS INSTITUTE OF TECHNOLOGY

June 2011

Author .....
Department of Materials Science and Engineering
May 11, 2011

Certified by .....
Marc Baldo
Associate Professor
Thesis Supervisor

Certified by .....
Harry L. Tuller
Professor of Ceramics and Electronic Materials
Thesis Supervisor

Accepted by .....
Christopher Schuh
Chair, Department Committee on Graduate Students

Chromium (III), Titanium (III), and Vanadium (IV) Sensitization of Rare Earth Complexes for Luminescent Solar Concentrator Applications

by

Nicholas John Thompson

Submitted to the Department of Materials Science and Engineering
on May 11, 2011, in partial fulfillment of the
requirements for the degree of
Master of Science in Materials Science and Engineering

Abstract

High optical concentrations without excess heating in a stationary system can be achieved with a luminescent solar concentrator (LSC). Neodymium (Nd) and ytterbium (Yb) are excellent infrared LSC materials: inexpensive, abundant, efficient, and spectrally well-matched to high-performance silicon solar cells. These rare earth ions are reasonably transparent to their own radiation and capable of generating high optical concentrations. Neodymium's and ytterbium's disadvantage is their relatively poor absorption overlap with the visible spectrum. Transition metals such as chromium (Cr), titanium (Ti), and vanadium (V) have broadband absorption covering the visible and near-infrared and can efficiently sensitize neodymium and ytterbium through a non-radiative energy transfer process.

Chromium, titanium, and vanadium containing glasses were fabricated using a custom designed glass making furnace. The optical properties including molar absorption coefficient, photoluminescence spectrum, and energy transfer characteristics were investigated to determine the suitability for LSC applications. Glasses containing Cr or V co-doped with Nd or Yb demonstrated energy transfer from the transition metal to the rare earth, a fundamental step toward integration into a LSC. Titanium co-doped glasses did not exhibit photoluminescence or energy transfer. Chromium co-doped glasses exhibit both forward and backward energy transfer. Vanadium holds the best promise as a sensitizer for LSC applications.

Thesis Supervisor: Marc Baldo
Title: Associate Professor

Thesis Supervisor: Harry L. Tuller
Title: Professor of Ceramics and Electronic Materials

Dedication

To my loving and supportive wife. My path to sucess has been filled with little steps and you have been my support through all of them. Thank you.

Contents

List of Figures

List of Tables

Chapter 1

Introduction

1.1 Thesis Outline

Sensitized luminescence of rare earth complexes by transition metals in an inorganic glass is an appealing materials platform for building a generation of luminescent solar concentrators focused on harvesting visible and near-infrared photons. Sensitized luminescence offers the potential to increase the absorption efficiency of the luminescent solar concentrator (LSC) while decreasing self-absorption losses. Transition metal complexes have broad-band absorption that spans from the visible into the near infrared, while rare earth complexes have high photoluminescence efficiency that is spectrally well matched to the bandgap of Si photovoltaic (PV) cells making them ideal candidates for near-infrared harvesting LSCs. Realization of a transition metal sensitized rare earth LSC starts with the characterization of the optical properties of the transition metal and rare earth doped glasses. This thesis will focus on chromium (Cr), titanium (Ti), and vanadium (V) transition metal elements and neodymium (Nd) and ytterbium (Yb) rare earth elements for their applications in luminescent solar concentrators based on Si PV cells.

Chapter one addresses the relevant background information on sensitized lumi-

nescence, luminescent solar concentrators, and ligand field theory. The efficiency of a planar LSC with only one luminescent center will first be defined; then, the more complex case of sensitized luminescence will be discussed. This discussion will be followed by a brief introduction to ligand field theory to explain optical transitions in transition metal and rare earth oxygen ligand complexes.

Chapter two describes the experimental details of sample fabrication and optical characterization. Experimental equipment and procedures necessary for synthesizing the glass samples are described. A short introduction for each optical characterization technique is given and relevant results from each technique are reported.

Chapter three discusses the experimental results bearing in mind relevant literature. The work with Cr attempting to overcome back energy transfer between Cr and Nd by cascading the energy to Yb was unsuccessful. We conclude that Cr sensitization of Nd or Yb is a low efficiency process in a phosphate glass matrix. Experiments to determine the usefulness of Ti (III) as a sensitizer demonstrated that it is fundamentally flawed even though previous literature suggests otherwise. Instead, V (IV) showed great promise as a sensitizer; its spectral characteristics are well suited for a Si photovoltaic cell and energy transfer to Nd or Yb activators is demonstrated for the first time.

1.2 Sensitized Luminescence

Sensitized luminescence as defined by Dexter[1], " refers to the process whereby an impurity atom (activator) having no appreciable absorption band in a given region of the spectrum is made to emit radiation upon excitation in this region as a result of absorption by and transfer from another impurity atom (sensitizer)." Dexter's terminology of sensitizer and activator will be used throughout this work.

The methods of energy transfer fall under one of two categories: radiative or

non-radiative. Radiative energy transfer is generally less efficient than non-radiative energy transfer and for LSC applications should be avoided since additional emission events increase the photon loss from the escape cone. This work will focus on non-radiative energy transfer, and as such, non-radiative energy transfer should be assumed unless specified otherwise. The theoretic aspects of non-radiative energy transfer are well characterized by Dexter [1] and Forster [2], and the reader is referred to those texts for additional information regarding the process. If the rate of energy transfer from the sensitizer to the activator is considerably faster than the non-radiative rate of the sensitizer, high energy transfer efficiencies are possible. If the energy transfer reaches unity, then the absorption spectra of the activator essentially become equivalent to that of the sensitizer; or in turn, the photoluminescence quantum efficiency (PLQE) of the sensitizer becomes that of the activator. The ability to boost the PLQE of the sensitizer in transition metal sensitizer/rare earth activator luminescent solar concentrators is significant since transition metals in amorphous hosts commonly have low PLQEs.

1.3 Luminescent Solar Concentrator

1.3.1 Luminescent Solar Concentrator Operation

Luminescent solar concentrators are a technology originally pioneered in the late 1970's by Weber and Lambe [3] and expanded in the 1980's by a myriad of authors. The technology gained notoriety again in the last five years with several high profile publications [4, 5].

The advantage of the LSC is that it decouples the processes of light capture/manipulation and charge conversion. This is advantageous since each process relies on different materials properties to be efficient. A generic luminescent solar concentrator device consists of a waveguide, luminescent material(s), and a photovoltaic (PV) cell as fea-

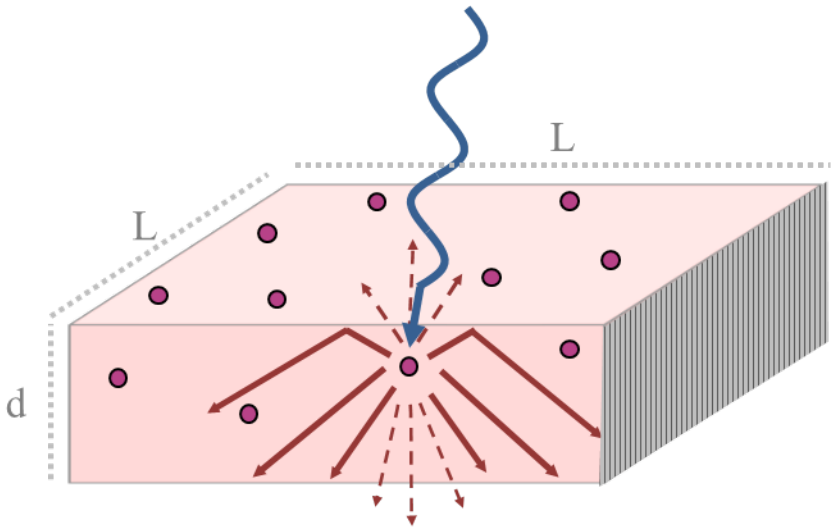

Figure 1-1: Basic luminescent solar concentrator structure: a luminescent species absorbs the incident photon and isotropically emits a stoke's shift photon which is waveguided to the solar cell. Normally photovoltaic cells are mounted on all four edges, but only one is shown for clarity.

tured in Figure 1-1. The concentration of light is attained by spatial redirection and geometry. For a LSC, light redirection is accomplished by absorption of the incident photon and isotropic re-emission of a stoke's shifted photon. Concentration of the photon flux is achieved when one dimension (d) of the waveguide is considerably smaller than the other two (L). The ratio of the surface to the area of the PV cell is the geometric gain (G). For Figure 1-1 the G is $\frac{L}{d}$. The PV cell mounted at the edge of the waveguide converts the concentrated photon flux into charge.

1.3.2 Efficiency of a LSC

To understand the more complex LSC based on sensitized luminescence, it is useful to first analyze the efficiency of a simple LSC device featuring only one luminescent center. The discussion of LSC device efficiency follows the notation of Currie et al.[4] and Batchelder et al. [6, 7]. For details not covered in this discussion, the reader is referred to those references.

The external quantum efficiency (EQE) of a LSC is defined as the number of charges collected by the PV cells divided by the number of photons incident on the LSC. For a LSC consisting of only a single luminescent center in a glass plate, the EQE (η_{EQE}) can be broken into individual efficiencies from different functions of the LSC.

$$\eta_{EQE} = \eta_{PV} \cdot \eta_{Abs} \cdot \eta_{PL} \cdot \eta_{trap} \cdot \frac{1-r}{1 - r \cdot \eta_{PL} \cdot \eta_{trap} - \eta_{PL} \cdot \bar{r} \cdot (1 - \eta_{trap})} \tag{1.1}$$

Where η_{PV} is the efficiency of the PV cell at the wavelengths of emission, η_{Abs} is the fraction of incident solar radiation absorbed by the luminescent center in the plate, η_{PL} is the photoluminescence efficiency of the luminescent center, η_{trap} is the fraction of emitted photons trapped by the waveguide, r is the average probability of reabsorbing a luminescent photon, and $\bar{r}$ is the average probability of reabsorbing a luminescent photon within the escape cone. The average probability of reabsorbing a luminescent photon is commonly referred to as the self-absorption efficiency.

Several simplifications to η_{EQE} are possible since this work is focused on the optical properties of the glass plate rather than the entire LSC device performance. Dividing η_{EQE} by η_{PV} will give η_{LSC} which is the number of photons arriving at the glass plate edges divided by the number of photons incident on the LSC. For transition metals and rare earth complexes which have low molar absorption coefficients, the last term in the denominator of the self-absorption term will be insignificant and can be ignored. The efficiency of the LSC is then

$$\eta_{LSC} = \eta_{Abs} \cdot \eta_{PL} \cdot \eta_{trap} \cdot \frac{1-r}{1 - r \cdot \eta_{PL} \cdot \eta_{trap}} \tag{1.2}$$

Further, Batchelder [7] showed that the trapping efficiency for a LSC with a

waveguide of a single refractive index, n, in air is

$$\eta_{trap} = \frac{(n^2 - 1)^{\frac{1}{2}}}{n} \tag{1.3}$$

The refractive index of the phosphate glass will be considered constant, even though it will vary slightly for changes in composition and equal to 1.51 [8]. Using Equation 1.3 the trapping efficiency is 0.749.

1.3.3 Efficiency of a Sensitized LSC

From Equation 1.2 three remaining terms should be discussed in more detail: η_{Abs}, η_{PL}, and r. Furthermore, it is especially important to analyze these terms in a sensitized LSC.

Absorption Efficiency

The absorption efficiency of a LSC with only one luminescent species can be calculated using Beer's Law: Equation 1.4.

$$\frac{I}{I_0} = \exp\left[-\alpha(\lambda) \cdot d\right] \tag{1.4}$$

$$\eta_{Abs} \equiv 1 - \frac{I}{I_0} = 1 - \exp\left[-\alpha(\lambda) \cdot d\right] \tag{1.5}$$

where I is the intensity of the light after passing through the sample of thickness d (cm), I_0 is the intensity of light incident on the sample, and $\alpha(\lambda)$ is the wavelength dependent absorption coefficient (cm^{-1}). Using this notation the absorption coefficient is dependent on the concentration of the luminescent center in the LSC. A more general measure of the absorption efficiency uses the molar absorption coefficient or

molar absorptivity, $\epsilon(\lambda)$, which is defined as

$$\epsilon(\lambda) \equiv \frac{\alpha(\lambda)}{c} \tag{1.6}$$

where $\epsilon(\lambda)$ has units of liter per mol centimeter, c is the concentration in moles per liter. Beer's Law becomes

$$\frac{I}{I_0} = \exp\left[-\epsilon(\lambda) \cdot c \cdot d\right] \tag{1.7}$$

and for a LSC without a reflective backing, η_{Abs} is

$$\eta_{Abs} = 1 - \exp\left[-\epsilon(\lambda) \cdot c \cdot d\right]$$

For a sensitized luminescent system, η_{Abs} needs to be redefined since the molar absorptivity of the sensitizer $\epsilon_S(\lambda)$ is not equal to the molar absorptivity of the activator $\epsilon_A(\lambda)$. Further, the concentrations of the sensitizer c_S and activator c_A in the LSC are independent, resulting in η_{Abs} for a sensitized luminescent system being defined as:

$$\eta_{Abs} = 1 - \exp\left[-(\epsilon_S(\lambda) \cdot c_S + \epsilon_A(\lambda) \cdot c_A) \cdot d\right] \tag{1.8}$$

The absorption efficiency parameter can be effortlessly tuned by choice of sensitizer or activator material, concentration of each species, and the thickness of the LSC.

Photoluminescence Efficiency

The PLQE for a single luminescent center LSC can be measured and is fixed value. However, for a sensitized LSC, it can be more complex. For example, the luminescent efficiency of photons absorbed by the sensitizer but emitted by the activator will be

$$\eta_{PL} = \eta_{PL_A} \cdot \eta_{transfer}$$

The concept that the η_{PL} will depend on whether the sensitizer or activator absorbs the radiation can be generalized. For a single activator and sensitizer:

$$\eta_{PL} = \frac{\int_0^\infty \{\eta_{PL_A} \cdot \epsilon_A(\lambda) \cdot c_A + \eta_{transfer} \cdot \eta_{PL_A} \cdot \epsilon_S(\lambda) \cdot c_S\} d\lambda}{\int_0^\infty \{\epsilon_A(\lambda) \cdot c_A + \epsilon_S(\lambda) \cdot c_S\} d\lambda} \tag{1.9}$$

For wavelength regions where the sensitizer has strong absorption relative to the activator Equation 1.9 will become $\eta_{transfer} \cdot \eta_{PL_A}$. For wavelengths where the activators absorption is strong Equation 1.9 will reduce to η_{PL_A}. If the sensitizer has broadband absorption but low $\eta_{transfer}$ it is clear that η_{PL} will be greatly reduced, which in-turn will limit the overall LSC performance.

Self-absorption Losses

The self-absorption term is an extremely important factor in LSC optimization that determines the practical limits on geometric gain of the LSC. Two loss processes occur when a luminescent photon is self-absorbed. First, a new photon may not be emitted if η_{PL} is less than unity. If another photon is emitted, probability of being captured by the waveguide is limited to the trapping efficiency. To begin understanding how to limit self-absorption, the definition of r is important. For a one dimensional LSC

$$r = \int_0^\infty f(\lambda) \cdot (1 - \exp[-l \cdot c \cdot \epsilon(\lambda)])\ d\lambda \tag{1.10}$$

where $f(\lambda)$ is the wavelength dependent photoluminescence normalized such that

$$\int_0^\infty f(\lambda) d\lambda = 1$$

and l is the length over which a photon must travel to reach the edge of the device. To re-iterate because the concept is important, in r the molar absorption coefficient will be the addition of the molar absorption coefficient for both the sensitizer and the

activator. If the sensitizer absorbs photons emitted by the activator, self-absorption losses will be large.

Equation 1.10 is directly from Batchelder et al. [6] and has several simplifications built in, including the geometry of the device and the broadening mechanisms for the absorption and photoluminescence curves. A more detailed look at how the geometry of the device affects r is explored by both Batcheleder et al. [6, 7] and Currie et al. [4]. However, Equation 1.10 highlights the critical aspect of self-absorption loss; the greater the overlap of the molar absorption coefficient and photoluminescence curves, the greater the reduction in the self-absorption efficiency.

1.3.4 Motivation for a Transition Metal Sensitized LSC

The use of sensitizers for rare earth activators is not a new and pioneering work in the 1980s [9, 10, 11, 12, 13] focused on the Cr-Nd and U-Nd sensitized systems. Although the original work on Cr in the 1980s was fairly extensive, there are large discrepancies in the Nd and Cr PLQEs reported by Reisfeld et al. in 1985 [10] and those reported by Jezowska-Trzebiatowska et al. [11] one year later for similar phosphate glass compositions. Work on the fabrication of tunable transition metal glass lasers spanning from the late 1980's to the early 2000's [14, 15, 16] demonstrated Ti(III) and V(IV) oxide complexes having promising optical properties for use in sensitized LSCs. These transition metals have yet to be explored as suitable sensitizers for rare earth ions for LSC applications.

1.4 Ligand Field Theory and Crystal Field Theory

A metal complex is composed of a central metallic element that is symmetrically coordinated by a ligand. A ligand can be an element or a compound, for example oxygen or CO. Ligand field theory is a method that uses molecular orbital theory to

calculate the electronic levels of the metal complex based on hydrogen like wavefunction interactions. Crystal field theory is a simplified version of ligand field theory that treats each ligand as a point charge and calculates the change in energy of the electronic states of the metallic element due to the electrostatic interactions with the ligands. Crystal field theory will be used to explain optical transitions for metals complexes with partially filled d and f valance shells.

1.4.1 Metallic Elements with d and f Valance Electrons

Transition metal and rare earth ion valance shells are composed of unfilled d or f orbitals respectively. In free space each orbital of the d or f shell will be equal in energy, even though it has a different spatial orientation. However, if the ion surrounded by spatially symmetric negative charges the degeneracy of the d or f shell orbitals is broken. The orbitals pointing towards the negative charges will increase in energy while those that point between them will not, creating electronics states that the valance electron can transition between. Quantum mechanical selection rules forbid electronic transitions between orbitals with the same angular momentum. However, the process of breaking the degeneracy of the d or f orbitals also mixes the angular momentum of the orbital with the ligand orbital that it is interacting with, thus relaxing the quantum mechanical selection rules. In general the orbital mixing is small leading to slow transition rate between states. Luminescent lifetimes for transition metal complexes are on the order of tens of microseconds while rare earth complex lifetimes are on the order of hundreds of microseconds to milliseconds. This does not mean that the transitions are low efficiency; the rare earth complexes often exhibit quantum efficiencies greater than 50%.

Optical transition for transition metal and rare earth complexes have very different line widths, which is a due to their valance structures. For transition metal complexes the valance shell is the d orbital with an empty n+1 s orbital and interactions with

the next nearest neighbor are great. However, for the rare earth complexes the n+1 s orbitals are filled, partially shielding the valance f electrons from interactions with next nearest neighbors. These differences create broadband absorption and emission for transition metal complexes and narrower band absorption and emission for rare earth complexes.

Chapter 2

Experimental Procedures

This chapter outlines the experimental procedures undertaken to form and characterize the transition metal and rare earth impregnated phosphate glass. The glass matrix is a ternary alloy of P_2O_5 -Al_2O_3 -K_2O where P_2O_5 is the glass forming oxide and Al_2O_3 and K_2O are networking modifying oxides. The transition metal or rare earth concentrations are between 0-2 mol %.

2.1 Glass Making Procedure

The glass making process followed the traditional melt-quench method, starting with the precursor compounds that decompose into the desired oxides. Although the melt quench method is seemingly easy to replicate, this author has found that simply stating the technique as the glass synthesis method is far from adequate to reproduce the complicated glass chemistry of a ternary glass. For example, the time a melt spends at its final temperature is often given as the only variable parameter of the melt quenching process. However, if the glass is melted under a controlled environment, it must be melted in a container that is subject to the same temperature as the melt. In many cases, the controlled environment is supplied by a silica or alumina cylindrical tube with a maximum manufacturer recommended temperature ramp rate of one to

two degrees Celsius per minute. Temperature rates greater than 5 °C per minute risk fracturing the tube. To bring a crucible filled with as-batched powders from 20 °C to 1200 °C at 2 °C per minute will require just under 10 hours of heating. When melting a volatile glass, like a phosphate glass, significant compositional changes can occur during the temperature ramping time as well as at the final melting temperature, making the temperature ramp rate an important synthesis parameter. Glass literature often only reports batched compositions and it was found that batched compositions can vary from the as-prepared compositions by up to ten atomic percent for higher melting temperature phosphate glass compositions.

2.1.1 Melt Quench Technique

Keeping in mind the desire for accuracy and reproducibility, being more articulate about the exact processing of a glass melt become worthwhile. Starting materials of $KPO_3 \cdot H_2O$ (Sigma-Aldrich 99.995%), $AlPO_4$ (Alfa Aesar 99.99%), P_2O_5 (Alfa Aesar 99.99%), Al_2O_3 (Sigma Aldrich 99.99%), Nd_2O_3 (Alfa Aesar 99.999%), Yb_2O_3 (Alfa Aesar 99.998%), Ti_2O_3 (Sigma Aldrich 99.9%), Cr_2O_3 (Alfa Aesar 99.97%), and VO_2 (Sigma Aldrich 99.9%) were massed, mixed, and placed in an alumina or quartz crucible with purity greater than 99%. Two decomposition reactions were relied upon to provide the final ternary glass composition.

$$2AlPO_4 \longrightarrow Al_2O_3 + P_2O_5$$

$$2KPO_3 \cdot H_2O \longrightarrow K_2O + P_2O_5 + 2H_2O$$

The crucible was loaded into a custom designed vertical tube furnace, featured in Figure 2-1. The system uses an alumina tube and water cooled seals to form a gas tight seal which is connected to a gas mixing system capable of flowing hydrogen, carbon monoxide, nitrogen, and oxygen at rates up to 1000 standard cubic centimeters

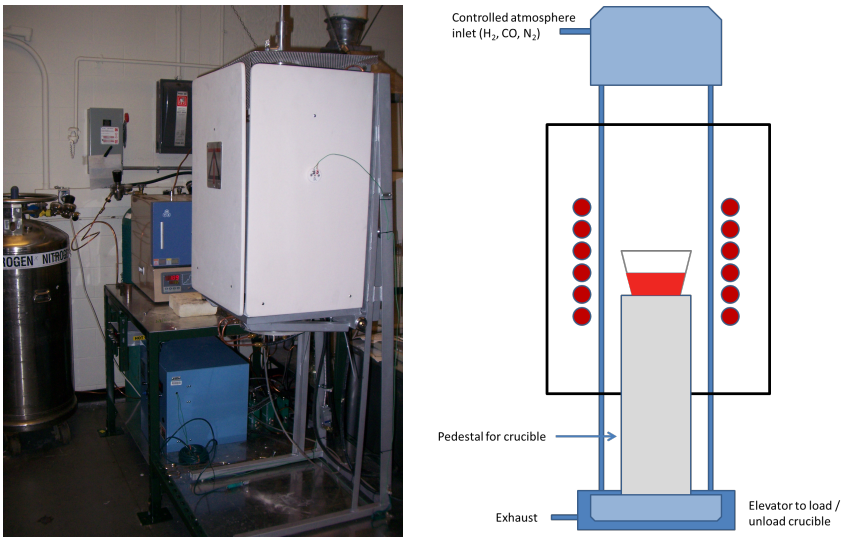

(a) Photograph showing the glass melting furnace, the annealing furnace, and the gas mixing system.

(b) Schematic diagram of the custom glass furnace depicting the furnace during operation.

Figure 2-1: Photograph, left, and schematic, right, of the custom designed vertical tube furnace.

per minute (sccm). At 1000 sccm the entire gas mixing system volume was replaced in under six minutes.

Two different glass melting ramp cycles were utilized. In the first, the sample was ramped at a controlled rate of 2.4 °C per minute up to 540 °C and then ramped at 2.7 °C per minute to the final melting temperature. In the second ramping routine, the samples were ramped at a controlled rate of 2.5 °C straight to the melting temperature. Additionally, a step of holding the sample at 300 °C for an hour to remove H_2O from the starting components was added to both ramping cycles and resulted in no additional volatilization. Once at the final melting temperature, the sample would be held there for 1 to 3 hours. Samples melted at higher temperatures were often covered to prevent volatilization of the P_2O_5.

With the glass melting process complete, the furnace was opened and the molten glass poured from the crucible onto a mold preheated to a temperature 20 °C above T_g. The mold and sample were immediately returned to the annealing furnace and

held at an annealing temperature for several hours and then cooled at a set rate to room temperature. Mold materials utilized included graphite, titanium, aluminum, and brass depending upon the desired annealing temperature and melt reactivity. The choice of mold material was never seen to change the bulk properties of the glass; although, improper mold material choice could cause the molten ingot to bind to the mold, preventing sample extraction. The annealed glass ingots were ground and polished to a sub-micron surface roughness on a polishing wheel. An average sample was circular with a radius of 25 mm and 1-5 mm thickness. Polished glass samples are featured in Figure 2-2.

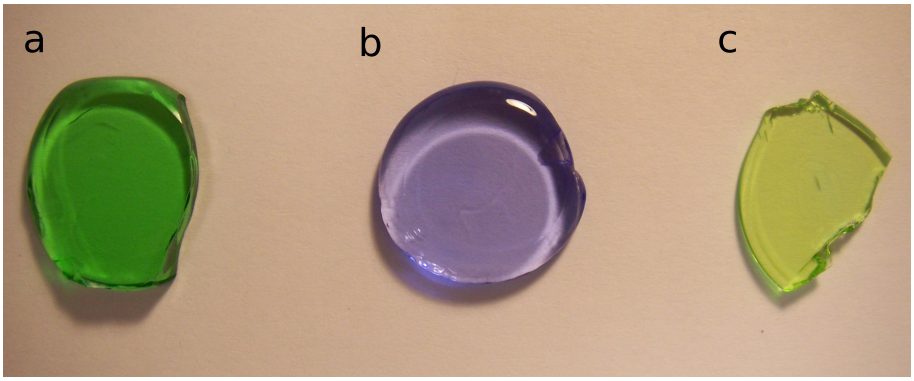

Figure 2-2: Photograph of a) Cr(III) doped phosphate glass b) Ti(III) doped phosphate glass c) V(IV) doped phosphate glass.

2.2 Chemical Characterization

Measurements of the composition and chemistry of the phosphate glass samples were made using X-ray Photoelectron Spectroscopy (XPS) on a Kratos Axis Ultra with a delay line detector and a monochromatic K-α Al x-ray source (1486.7 eV). Additionally, several samples were sent out for independent analysis using Proton Induced X-ray Emission (PIXE). The compositions measured by XPS and PIXE were in agreement. X-ray diffraction was used to determine if any crystallization occurred during

the glass forming process. No crystallites were observed in the intensity versus two theta scans indicating that any crystalline content was below the detection limit of the instrument.

2.2.1 X-ray Photoelectron Spectroscopy

X-ray photoelectron spectroscopy is a technique in which the sample is illuminated with high energy monochromatic x-rays to eject electrons from the nucleus and measure the kinetic energy of the emitted electrons. Plotting the number of electrons collected versus the kinetic energy of the electrons created a fingerprint for each element. From the XPS spectra, it is possible to identify the elements present in the sample, the relative amount of each element, and chemistry changes that each element experiences in the sample. Since the XPS process depends on accurately measuring the kinetic energy of the electron, the electron must only undergo elastic scattering processes before leaving the sample. For most materials, an electron will undergo inelastic scattering in approximately the first 10 nanometers, thus XPS is strictly a surface sensitive technique with an information depth from 1-10 nanometers.

For analyzing the glass, XPS was primarily used for composition analysis. Compositions of polished bulk specimens used for optical measurements were measured using XPS; however, these samples exhibited surface contamination of Zn and Na from the polishing process. Powdering the glass using a mortar and pestle removed the surface contamination issue. Reported compositions for samples were calculated from the ratio of the integration of the area under a peak for each element divided by the area under all element peaks, properly adjusting for different elemental and orbital sensitivities. To improve the accuracy of the measurement, low pass energy scans were made on the regions around the elements of the glass. A low pass energy retards the electron velocity, increasing the energy resolution and sharpening the peak shape, but sacrificing signal intensity.

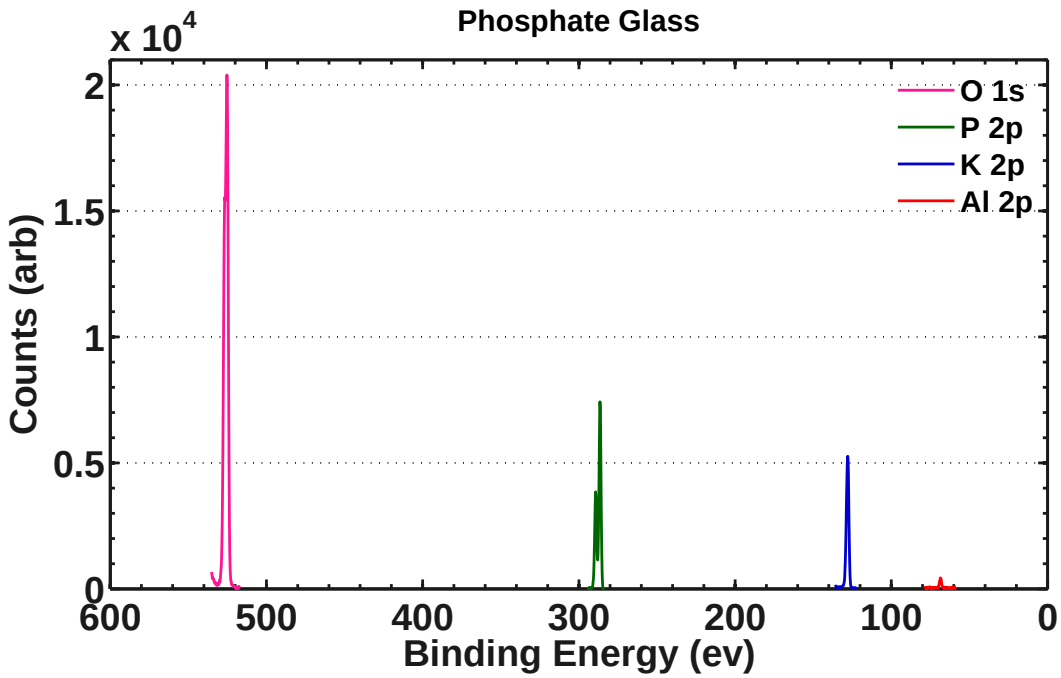

Figure 2-3: Overlay of high resolution XPS spectra of glass elements.

Figure 2-3 is a typical overlay of the low pass energy scans of each of the elements in the phosphate glass matrix. The baselines of individual scans were shifted to zero counts for clarity. A similar process was undertaken to remove the background before integrating for composition analysis. The composition of this particular sample is 63.9% O–21.6% P–3.7% Al–10.8% K atomic which corresponds to 60% P_2O_5 –10% Al_2O_3 –30% K_2O with error bars on the order of 1-2%.

2.2.2 X-ray Diffraction

To prove whether the glass samples had any crystallites, x-ray powder diffraction was performed using Cu K-α radiation. Figure 2-4 shows the Intensity vs. 2θ plot for each of the transition metal doped glasses. In all cases, no sharp crystalline peaks were observed, indicating that any crystalline content lies below the resolution of the instrument. Small shifts in the two theta value of the peak X-ray diffraction intensity

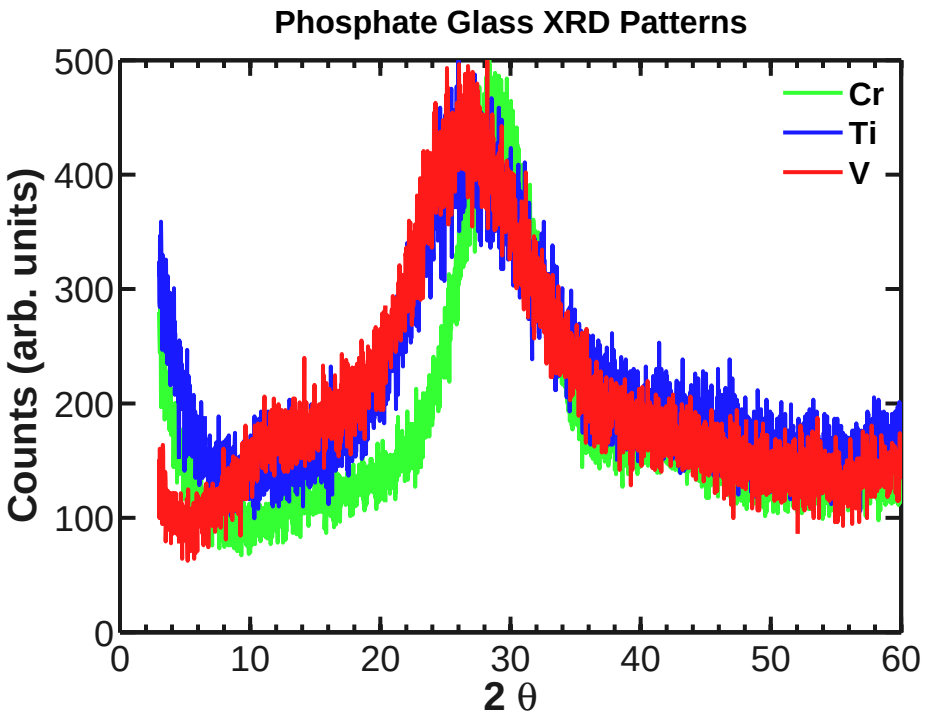

Figure 2-4: Intensity versus two theta scan for powdered phosphate glass.

may be due to sample preparation conditions rather than intrinsic differences between samples. The glass was powdered using a mortar and pestle, resulting in glass pieces larger than the depth of the sample holder, which could have resulted in small shifts of the peak in the Intensity vs. 2θ plot.

2.3 Optical Characterization

For LSC applications, it is especially important to characterize the absorption and luminescent properties of potential sensitizers and activators. This includes the wavelength dependence of the molar absorption coefficient, the wavelength dependence of the emission, and the emission efficiency. Additionally, in sensitized luminescent systems, the non-radiative energy transfer process is important to study.

2.3.1 Absorption

Absorption measurements in the visible and NIR regions were performed using a Pro-Optics Aquila nkd-8000. The instrument used a fixed angle of incidence and measured transmission (T) and reflection (R) relative to a reference quartz slide. Using the transmission and reflection, it was possible to calculate the molar absorption coefficient discussed in Chapter 1, Equation 1.7.

$$I = T$$

and

$$I_0 = 1 - R$$

it is found that

$$\frac{I}{I_0} = \frac{T}{1-R} \tag{2.1}$$

substituting into Equation 1.7 and solving for ϵ one obtains

$$\epsilon = \frac{-\ln[\frac{T}{1-R}]}{t \cdot c} \tag{2.2}$$

The molar absorption coefficient for Cr(III), Ti(III), V(IV), Nd(III), and Yb(III) as a function of wavelength are plotted below. For those used to thinking in terms of absorption coefficient, simply multiply the molar absorptivity by the concentration reported in the caption. It is important to note two observations. First, the strength of the optical transitions is weak. For example, the peak absorption coefficient for a V glass with a concentration of 0.09 moles per liter at 698 nm is 2.7 cm^{-1}, while the absorption coefficient in a direct band-gap semiconductor is 10^5-10^6 cm^{-1}. Secondly, the transition metal ions exhibit much broader absorption lines than the rare earth ions, which is consistent with the oxygen ligand field perturbing the d orbital to a great extent than the shielded f orbital.

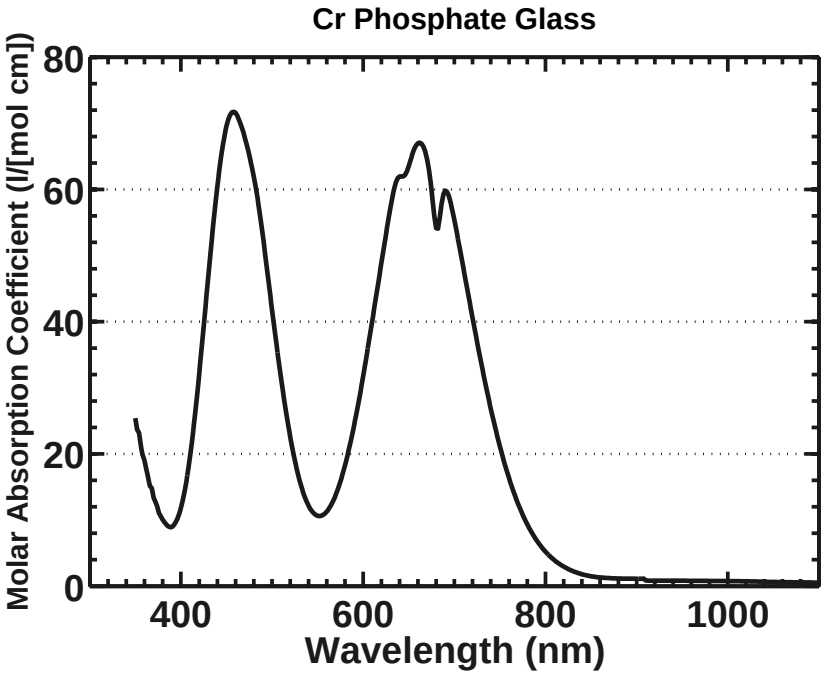

Figure 2-5: Molar absorptivity for Cr(III) with a concentration of 0.04 moles per liter.

2.3.2 Photoluminescence

Photoluminescence (PL) is the process under which a photoactive material emits a photon after being excited by an incident photon. Characterization of the PL spectrum is very important in LSC materials since self-absorption plays a large role in device performance. A PL spectrum for each of the luminescent transition metals is reported below. The emission for the rare earth complexes are very similar to those previously reported in the literature, since the f orbital is not significantly perturbed by the ligand field. Representative PL spectra of the rare earth ions are visible in the co-doped systems and will not be individually reported. The spectral shape for each ion is the same in different composition phosphate glasses, although the position of the maximum emission shifts for large composition changes, as featured in Figure 2-10.

Photoluminescence spectra were acquired using a spectrophotometer with a Si

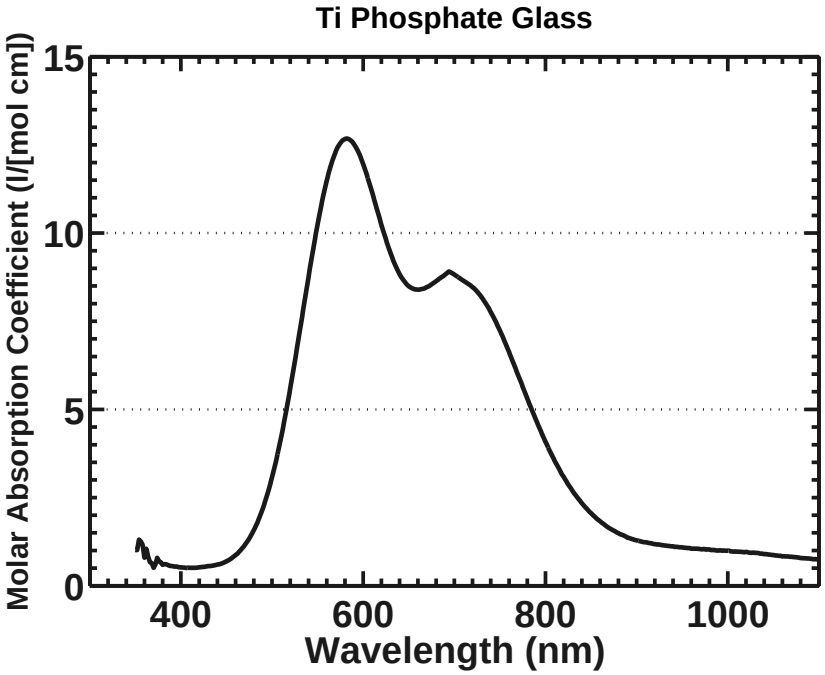

Figure 2-6: Molar absorptivity for Ti(III) with a concentration of 0.10 moles per liter.

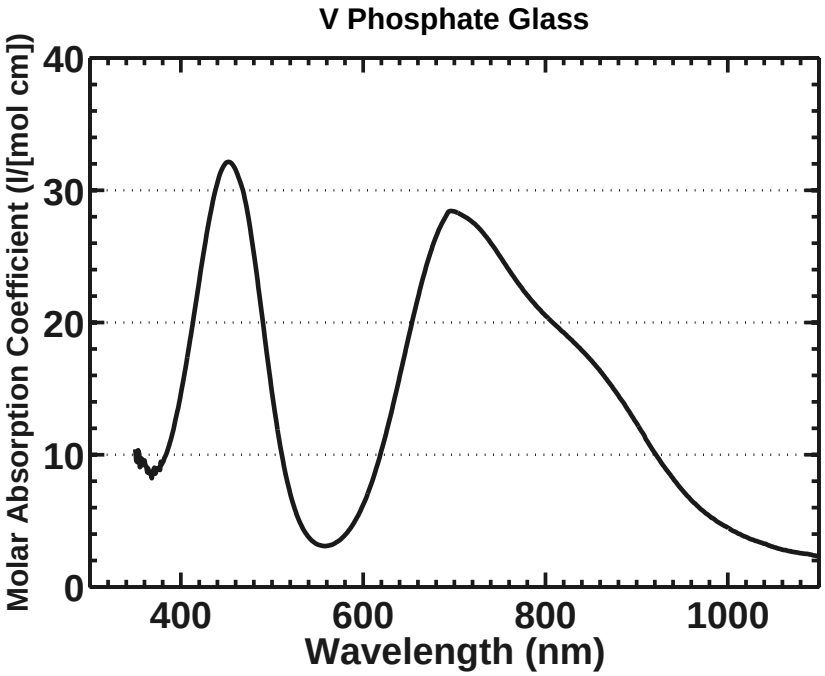

Figure 2-7: Molar absorptivity for V(IV) with a concentration of 0.09 moles per liter.

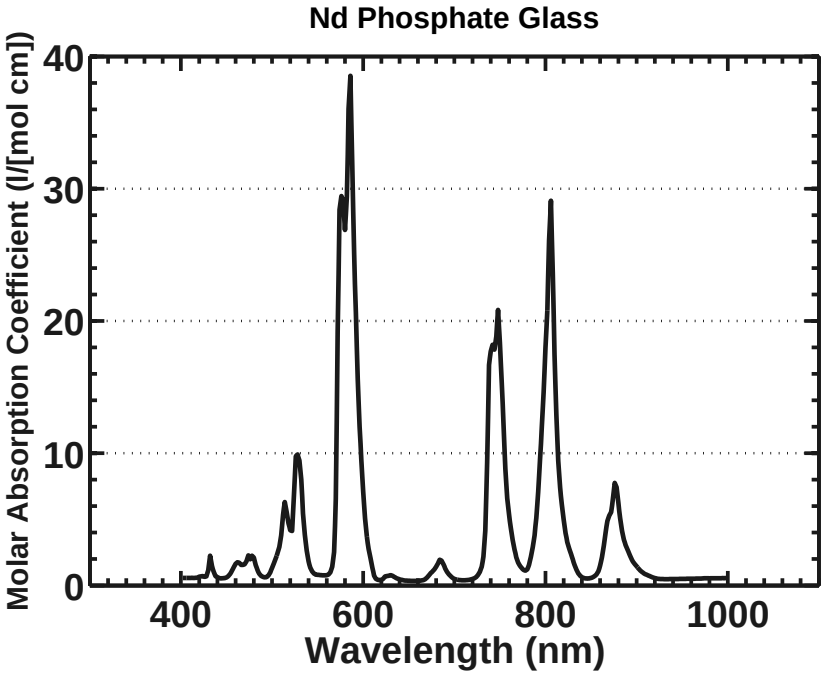

Figure 2-8: Molar absorptivity for Nd(III) with a concentration of 0.08 moles per liter.

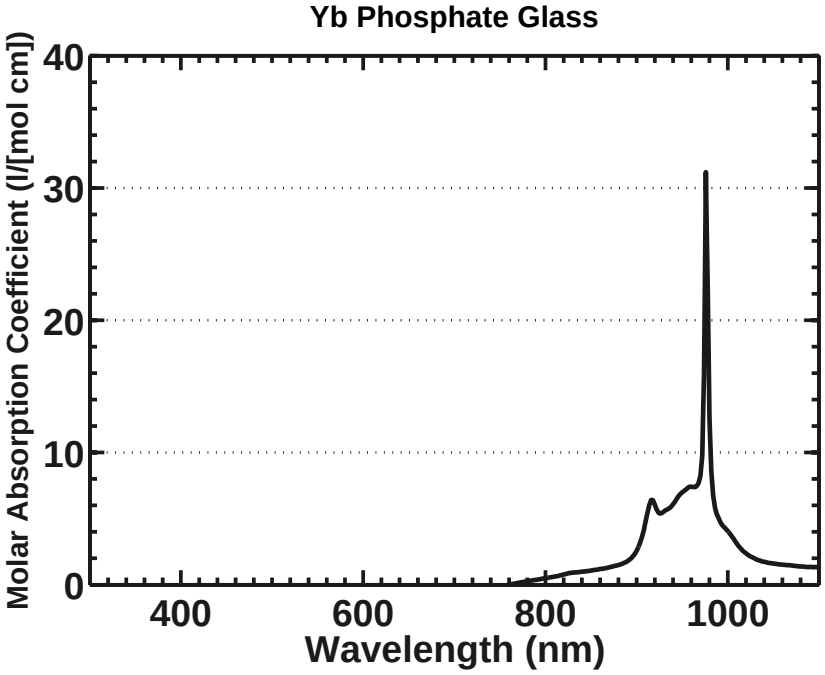

Figure 2-9: Molar absorptivity for Yb(III) with a concentration of 0.11 moles per liter.

CCD cooled to -30 °C. The excitation sources were lasers passed through a filter to any extraneous laser emission in the region of the sample emission. The emitted light from the sample face was focused by a lens through a filter to remove the scattered laser light and onto a multimode fiber which guided the light into the spectrophotometer. The optical set-up, including the lens and filter, was calibrated using a tungsten light source approximating the shape of the bulb as a black body at 3300 Kelvin. The blackbody spectrum was fit using 8 free variables and the measured spectrum was divided by the fit spectrum to determine the correction file. One may notice that in the longer wavelength portions of the near-infrared there is more noise in the data and the PL signal does not fall off exponentially, as would be expected. This is an artifact of the Si charge coupled device (CCD) used to capture the spectra. Wavelengths greater than 1100 nanometers are extremely close to the bandgap of Si, the collection efficiency of the CCD is limited and even correcting for these inefficiencies does not fully compensate for the additional losses in the CCD.

In the PL spectra, the y-axis has been normalized to one for easier comparison of shape. The shapes of PL plots of the co-doped glasses are an indication of energy transfer in the co-doped systems. For example, there are clearly two contributions to the emission in Figure 2-11, one from Cr and another from Yb. It is important to note that the excitation wavelength was 635 nm, a value at which Yb has no absorption. In Figure 2-12 small differences in the emission spectrum can be seen depending on which ion was excited with the incident laser. There is a large contribution from Cr seen when Cr is directly excited and more contribution from Nd when Nd is primarily excited, with a 532 nm laser. In contrast, in Figure 2-16 there is only slight evidence of V PL in addition to Nd PL, visible from the non-zero emission for wavelengths between 940-1020 nm. A comparison of the relative contributions from Cr or V and the rare earth ions are addressed in great detail in Chapter 3.

For Figure 2-10 the emission is plotted for different composition glasses and the

sample number is used to reference the different spectra. Appendix A contains a table with the composition of all the samples measured using XPS. Compositions for each sample or an identically processed sample can be found there.

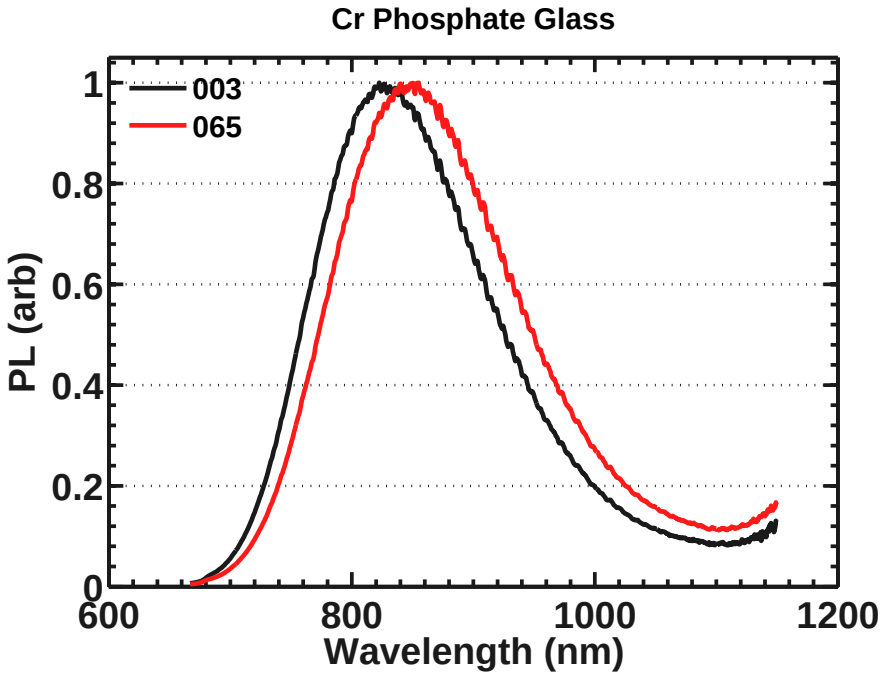

Figure 2-10: Facial emission of Cr phosphate glass under 635 nm excitation for two different glass compositions labeled 003 and 065.

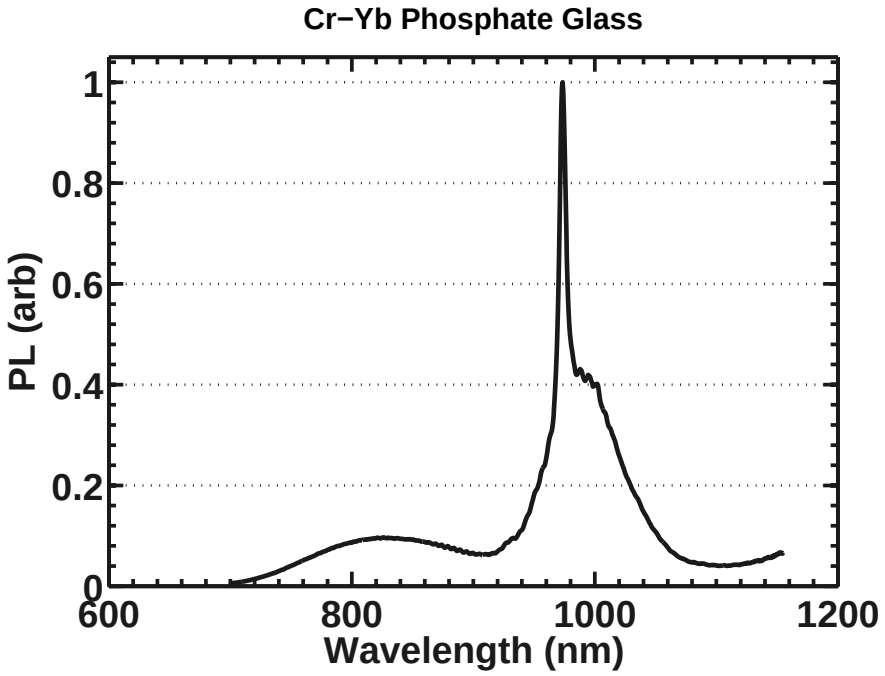

Figure 2-11: Facial emission of Cr-Yb co-doped phosphate glass under 635 nm excitation. There are two clearly distinguishable features, the broad peak from Cr and the sharp feature from Yb at 975 nm.

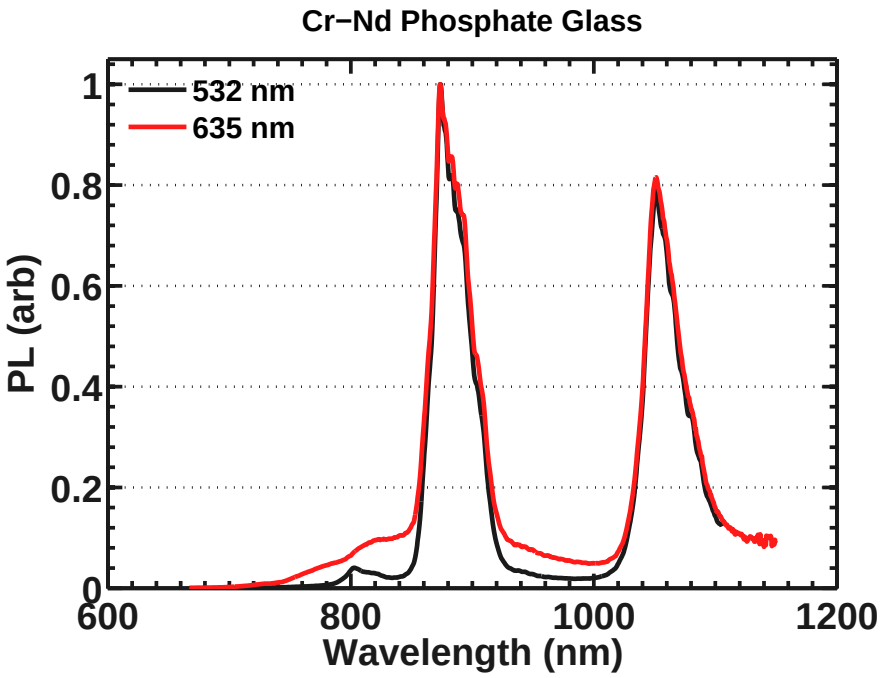

Figure 2-12: Facial emission of Cr-Nd co-doped phosphate glass under 532 and 635 nm excitation. The intensity of Cr emission increased when Cr was pumped directly with 635 nm light.

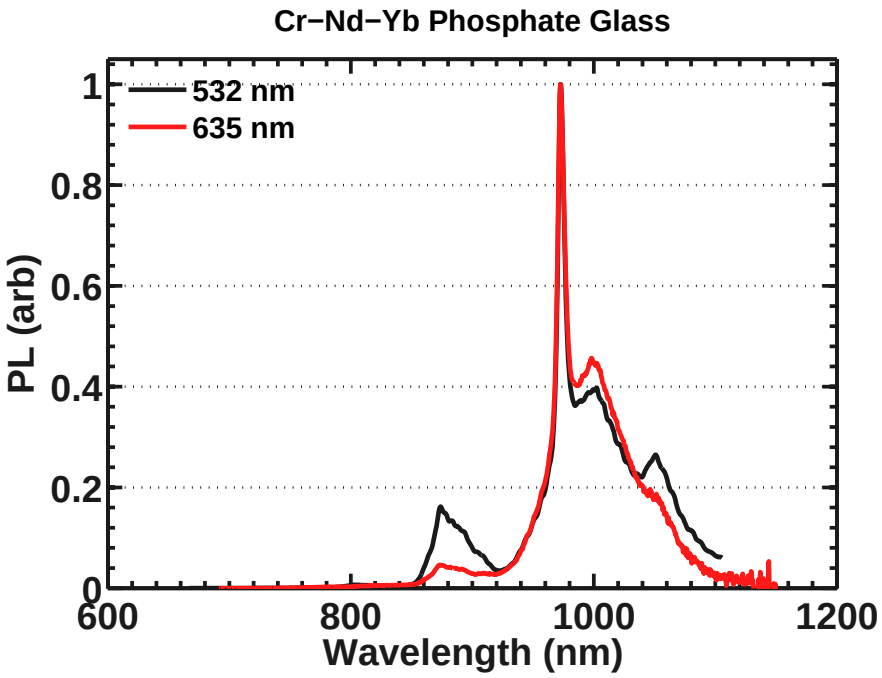

Figure 2-13: Facial emission of Cr-Nd-Yb tri-doped phosphate glass under 532 and 635 nm excitation. Notice the additional contribution from Nd when it was pumped directly with 532 nm light.

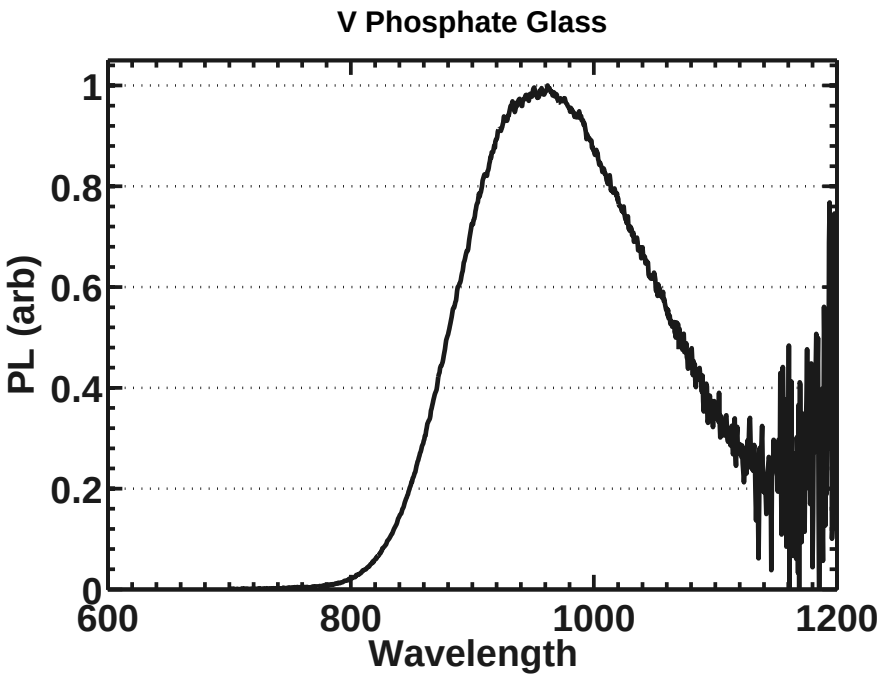

Figure 2-14: Facial emission of V phosphate glass under 635 nm excitation.

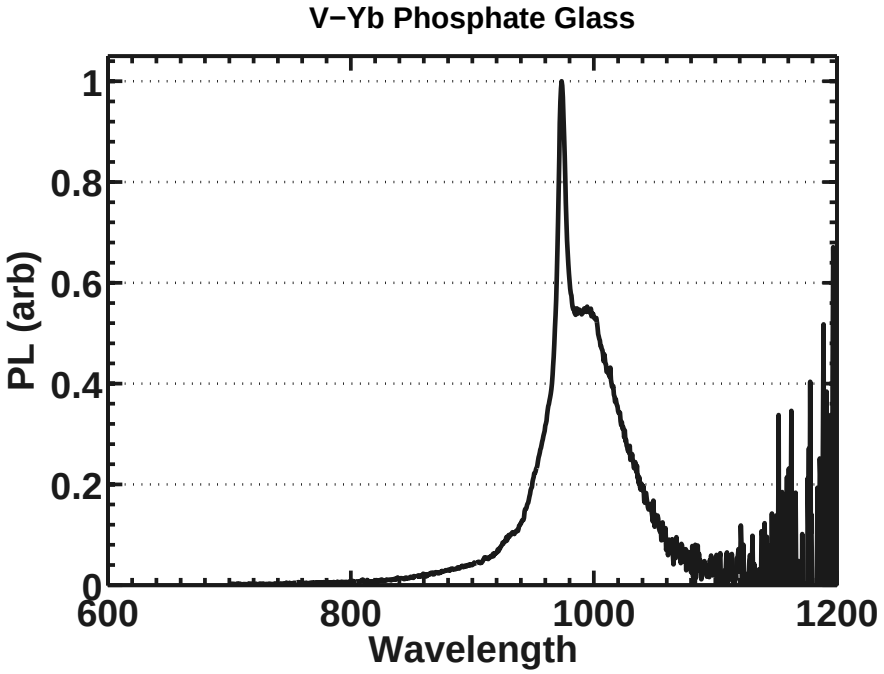

Figure 2-15: Facial emission of V-Yb co-doped phosphate glass under 635 nm excitation. There are two clearly distinguishable features, the broad peak from very low intensity V peak and the sharp feature from Yb.

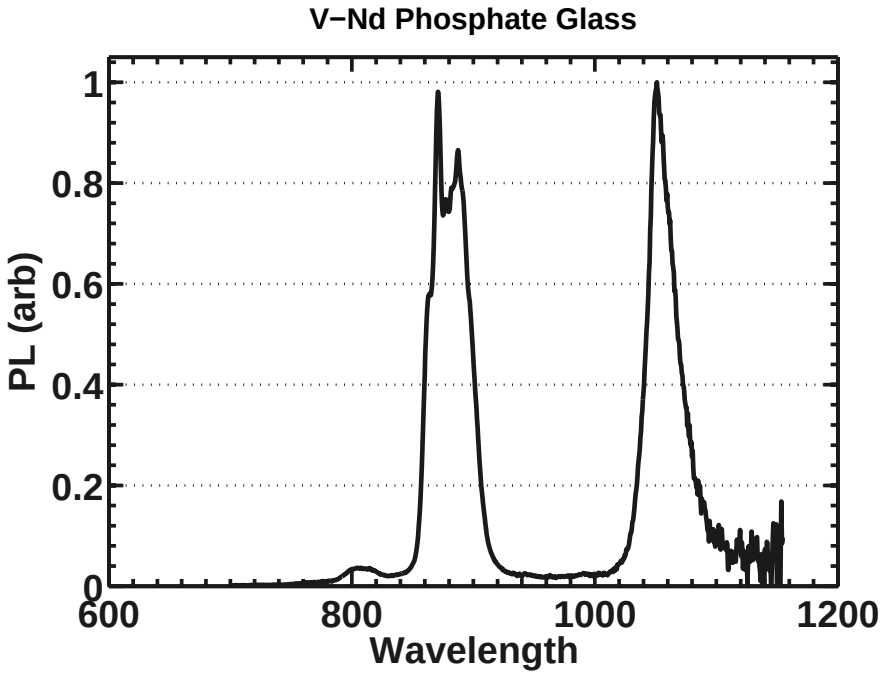

Figure 2-16: Facial emission of V-Nd co-doped phosphate glass under 635 nm excitation.

2.3.3 External and Optical Quantum Efficiency

The external quantum efficiency (EQE), defined as the number of photons out of the device divided by the number of photons incident on the device, is a very important parameter to measure. However, to characterize the efficiency of the photon processes, the optical quantum efficiency (OQE) is a more useful measurement. The OQE is defined as the number of photons emitted divided by the number of photons absorbed. Using the definition of EQE we can simply express the OQE as EQE in percent divided by the absorption in percent.

In general EQE and OQE are a function of wavelength. Logically, the luminescent species or sensitizers must absorb the photon before a photon can be emitted, barring excitation by another means. One should expect that the wavelength dependence of EQE should match the shape of the absorption spectrum, since absorbing more

photons should result in emitting more photons. Figure 2-17 demonstrates that the EQE traces the absorption spectrum; make sure to note the different values on the left and right vertical axes.

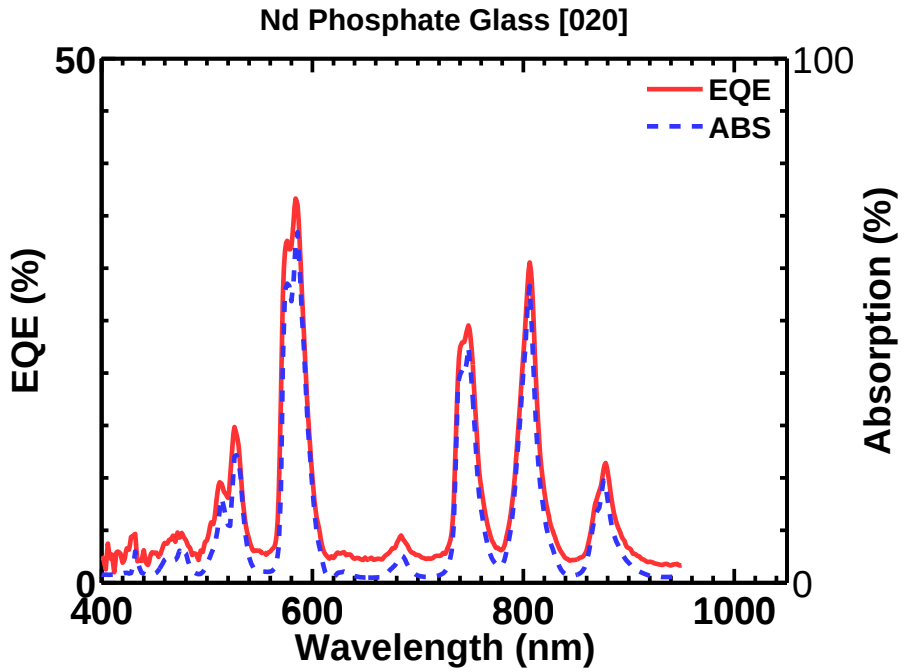

Figure 2-17: External Quantum Efficiency and Absorption of Nd phosphate glass, note the different scales on the vertical axes.

The EQE measurement is completed using an integrating sphere. An integrating sphere is a sphere with its interior walls coated in highly reflective material and whose entrance and exit ports allow for optical beams to probe the sample. The basic measurement necessary to obtain an EQE spectrum is shown in Figure 2-18. The sample is illuminated with a monochromatic beam, labeled λ_{pump} in Figure 2-18 and the transmitted and reflected beams leave the sphere through open ports. Emission from the sample was recycled by the sphere until it was absorbed by the photo detector. In an ideal system, the current measured by the photo detector is solely due to photons emitted by the sample. Careful characterization of the wavelength dependence of the absorption of the sphere coating allows one to correctly adjust for the photons lost to the sphere recycling process. Furthermore, the input beam is

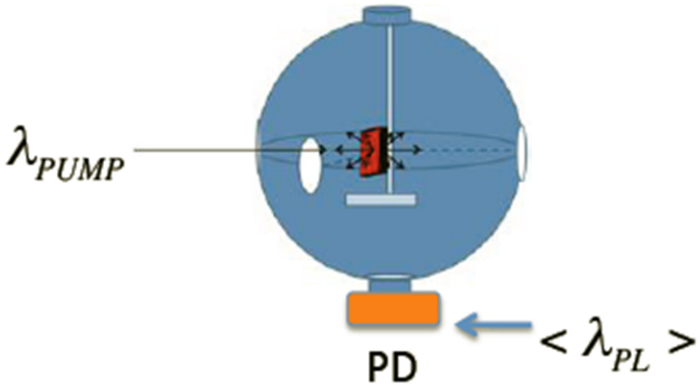

Figure 2-18: Diagram of primary measurement for determining an EQE spectrum. The reflected and transmitted beams exit the integrating sphere and only photoluminescence is collected by the photo detector (PD).

optically chopped and the photo detector current is measured using a lock-in amplifier to remove any background light sources.

The shape of the measured OQE plots was often not what one would expect from an ideal perspective. In the ideal case, the OQE plot would be flat and at a constant value equal to the photoluminescence quantum efficiency in regions where the ion absorbs and zero elsewhere. However, in non-ideal samples, scattering from small bubbles or from the surface of the sample resulted in photocurrent in regions in which the absorption was very small. Thus, when the EQE was divided by the absorption, it created a large value for the OQE. This is clearly seen in Figure 2-19. For wavelengths from 500-600 nm the OQE value became very large. This was not real but rather an artifact due to significant scattering over these wavelengths and little absorption. The important information contain in Figure 2-19 is that in regions of Cr absorption, the OQE was 2.4%. Table 2.1 summarizes the OQE data for each ion in singly, doubly, and triply doped systems.

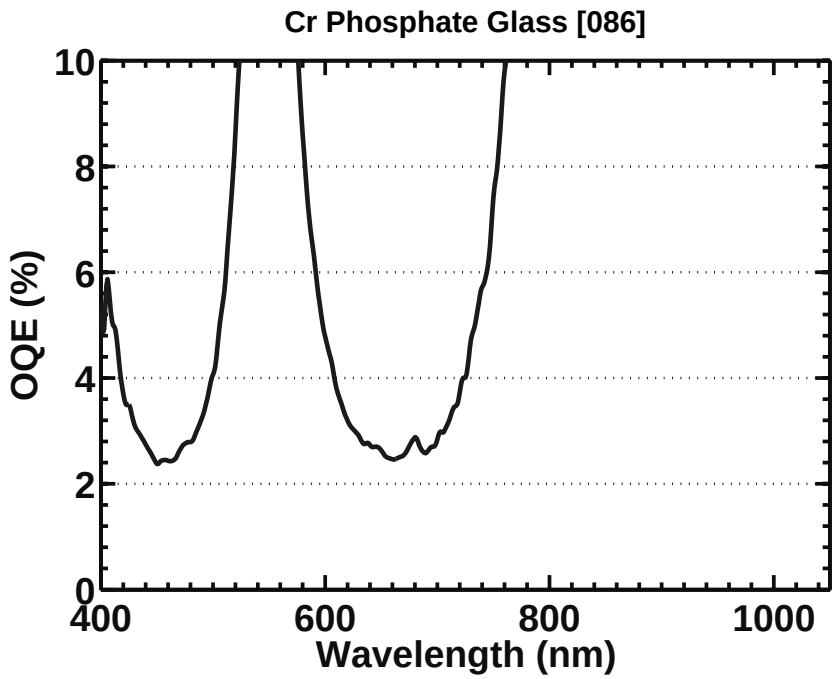

Figure 2-19: Optical Quantum Efficiency and Absorption of Cr phosphate glass.

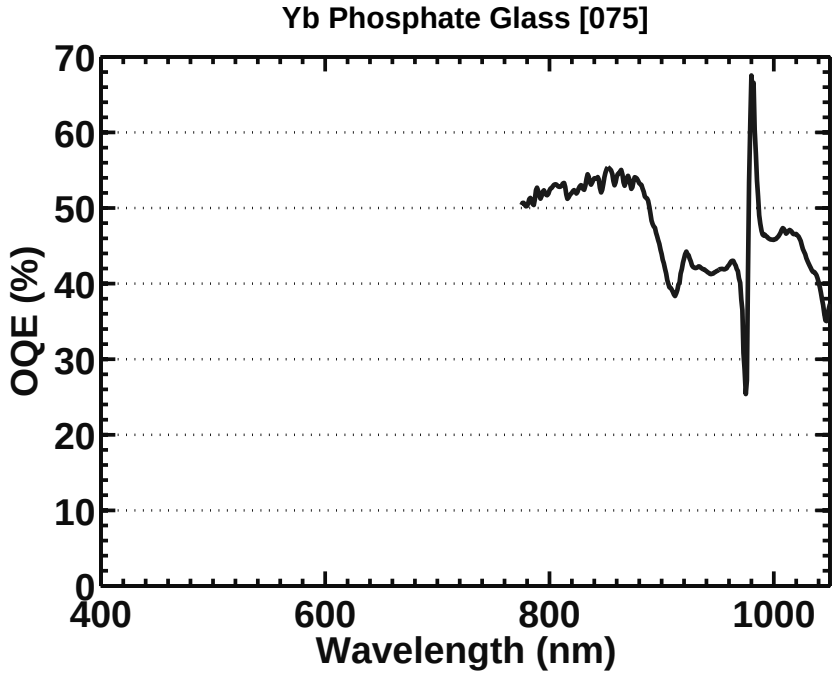

Figure 2-20: Optical Quantum Efficiency of Yb phosphate glass.

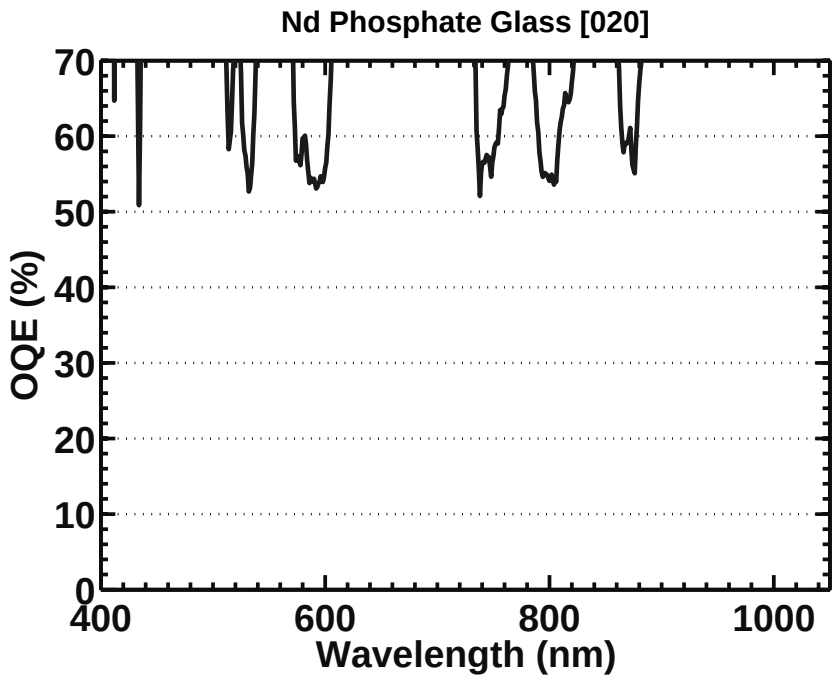

Figure 2-21: Optical Quantum Efficiency of Nd phosphate glass.

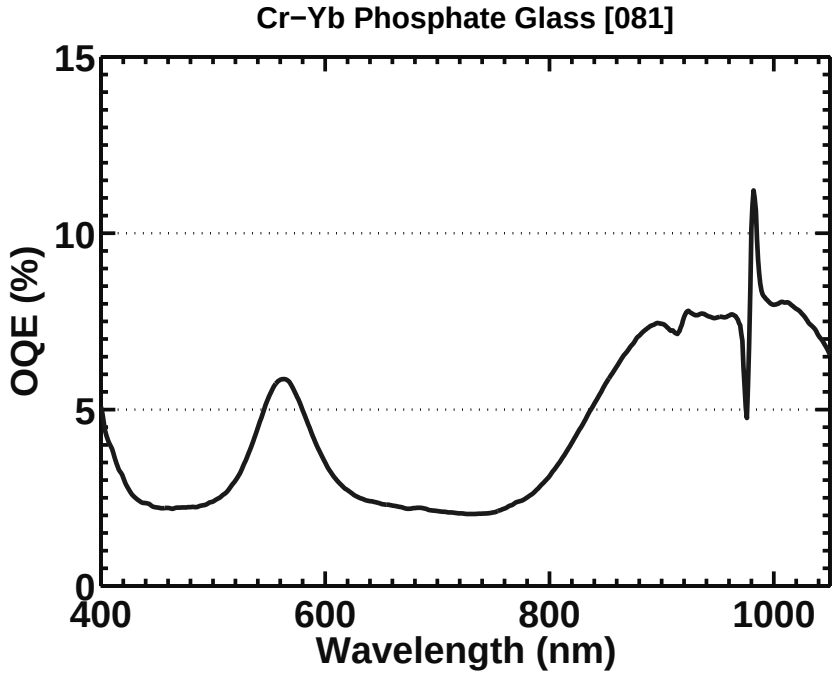

Figure 2-22: Optical Quantum Efficiency of Cr-Yb co-doped phosphate glass.

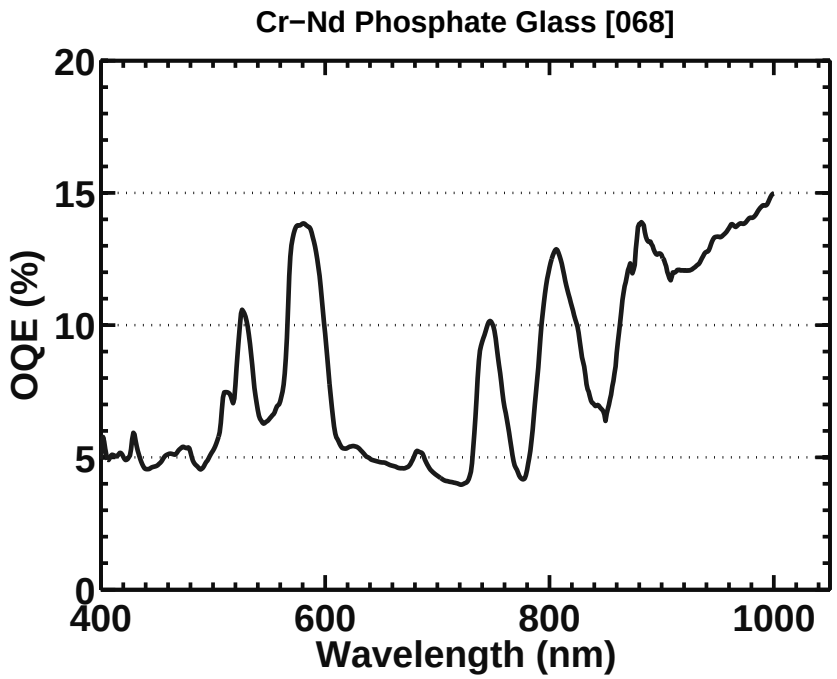

Figure 2-23: Optical Quantum Efficiency of Cr-Nd co-doped phosphate glass.

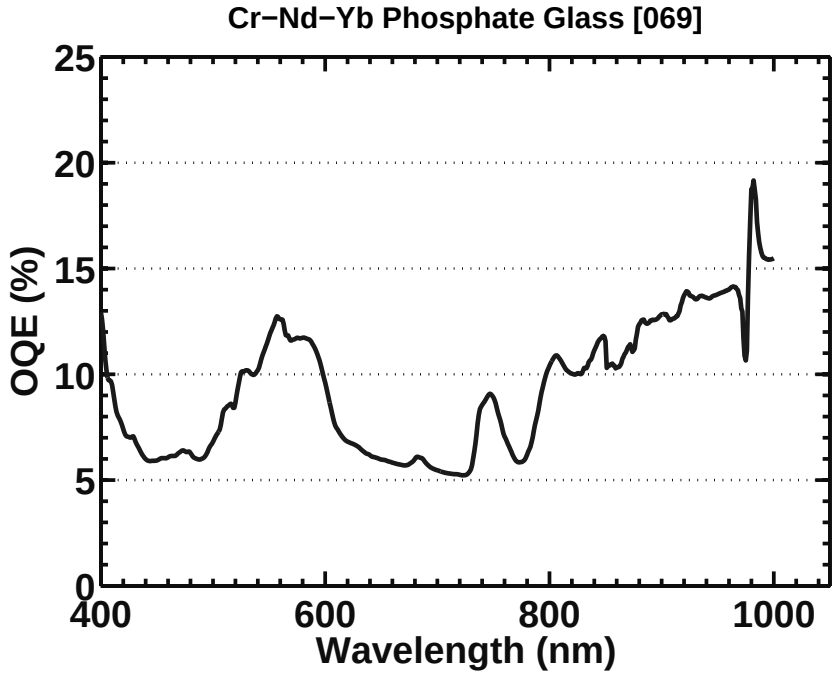

Figure 2-24: Optical Quantum Efficiency of Cr-Nd-Yb co-doped phosphate glass.

Table 2.1: OQE data for each ion in different singly, doubly, and triply doped systems.

Ion	**Ion Oxide (Mol %)**	**Doping Ions**	**OQE (%)**
Cr	0.120	Cr	2.4
Yb	0.365	Yb	45
Nd	0.352	Nd	55
Cr	0.260	Cr-Yb	2.2
Yb	0.390	Cr-Yb	7.5
Cr	0.117	Cr-Nd	5
Nd	0.830	Cr-Nd	10-14
Cr	0.116	Cr-Nd-Yb	6
Yb	0.730	Cr-Nd-Yb	10
Nd	0.855	Cr-Nd-Yb	13

Chapter 3

Chromium (III), Titanium (III), and Vanadium (IV) Oxides as Sensitizers

In Chapter 2, the molar absorptivity, photoluminescence, and OQE of Cr, Ti, V, and co-doped systems were measured. Now, it becomes important to discuss them in the context of applications to a sensitized LSC.

3.1 Chromium (III) Oxide

Chromium oxide exhibits broadband transitions between its 3d orbitals due to its ligand field splitting and offers great promise for sensitized LSCs. For Cr (III) in an octahedral environment, the ligand field creates two absorption bands: one spanning from 400-510 nm and the second from 600-800 nm as previously shown in Figure 2-5. Samples containing Cr-Nd, Cr-Yb, and Cr-Nd-Yb were fabricated to assess the application of Cr in sensitized LSCs. When illuminated with radiation primarily absorbed by Cr, each of the doped systems produced luminescence from the rare earth, with some residue Cr emission visible. This is evidence of forward energy

transfer occurring in these samples.

3.1.1 Literature Review: Cr (III) sensitization of Rare Earth Elements

As previously reported in the literature, sensitization of Nd with Cr has a fatal flaw: back energy transfer. To increase the efficiency of a sensitized LSC, the sensitization process should have the high PLQE element acting as the activator and the broadband absorbing element as the sensitizer. However, in the Cr-Nd system the Nd also acts as the sensitizer for Cr, donating its excited state energy to Nd in a process termed back energy transfer. Jezowska-Trzebiatowska et al. studied various ratios of Cr to Nd in a lithium phosphate glass, unsuccessfully attempting to determine a composition where back energy transfer was suppressed. From that study, the best Nd PLQE reported was 28% when co-doped with Cr, with no report of a quantum yield without Cr [11]. Recently, Mizuno et al. observed the same behavior in silicate glasses: the PLQE of a Nd doped glass is greater than 45% and is less than 6% when in a Cr-Nd co-doped glass [17]. Non-quantitative analysis of energy transfer using photoluminescence has also been carried out for the Cr-Nd and Cr-Yb systems by Reisfeld et al.[18].

Non-radiative Energy Transfer Cascade

Neuroth and Haspel [13] devised a thoughtful solution to the Cr-Nd back energy issue, they included Yb in a Cr-Nd co-doped glass. Ytterbium will act as the lowest energy state and ideally all the energy in the system will be funneled to it. The excited state on Yb being lower in energy than that on Nd, it was theorized that the efficiency of the back energy transfer process to Cr would be reduced. While they observed improvements in the excitation spectra, an EQE spectra not corrected for all inefficiencies of the optical system, upon adding Yb to the Cr-Nd co-doped silicate glass, they did not quantitatively measure any changes in the Nd PLQE upon the

addition of Yb.

3.1.2 Discussion of Observed Cr (III) Sensitization

As previous literature demonstrated for the Cr co-doped systems, we, too, found that the OQE of the rare earth elements was lowered upon the introduction of Cr. Neodymium's PLQE is reduced from 55% to around 13%, and for the first time, we quantitatively demonstrated the quenching effect is greater for Yb, with its PLQE going from 45% to 7.5%. We attribute the additional loss in OQE to a larger back energy transfer efficiency which is likely due to the longer photoluminescent lifetime of Yb, 450 μs, while neodymium's lifetime is 350 μs. Utilizing a tri-doped system of Cr-Nd-Yb increased the overall OQE of the Cr regions of absorption, which confirms Neuroth and Haspel's work. Further, the hypothesis that Yb will be the lowest energy state is confirmed by the photoluminescent spectra, which was dominated by Yb emission. However, doping with Yb does not appreciably increase the efficiency.

Quantification of the efficiency of the first energy transfer event is important to determine so that the efficiency of a system without back energy transfer can be estimated. Doing so requires detailed study of the IQE plots for co-doped system; we will use the Cr-Yb system as an example. It is important to remember that the OQE is the number of photons emitted divided by the number of photons absorbed. For simplicity, all emitted photons are assumed to be emitted by Yb. If no back energy transfer process existed, Yb would emit all photons absorbed, and the OQE in the regions of Yb absorption would simply be equal to the PLQE of Yb. For regions of solely Cr absorption, the OQE would be equal to the transfer efficiency times the Yb PLQE. Dividing the OQE spectra by the PLQE of Yb would yield a 100% in regions of Yb absorption and the energy transfer efficiency in regions of Cr absorption.

Coincidentally, the process described above also applies to a system with back energy transfer. By dividing the OQE spectra by the efficiency of Yb, including the

loss due to back energy transfer, the efficiency of the first energy transfer event from Cr to Yb can be determined. Figure 3-1 is the OQE plot from Figure 2-22 divided by the efficiency of Yb, 7.5% and multiplied by 100. The efficiency of the first energy transfer event from Cr to Yb is 28% and a similar analysis for Cr-Nd results in a 40% first energy transfer efficiency. The non-radiative energy transfer process has a $\frac{1}{r^6}$ dependence [**?**] and is highly contingent on the relative concentrations of the sensitizer and activator. The values for the first energy transfer efficiency were determined to provide a reference point for the energy transfer efficiency in a phosphate glass. We also demonstrate calculating the first energy transfer efficiency through a method that differs from the approach of Mizuno et al. who only uses the PLQE of the rare earth element to determine transfer efficiency [17]. Optimization of the first energy transfer event was not attempted.

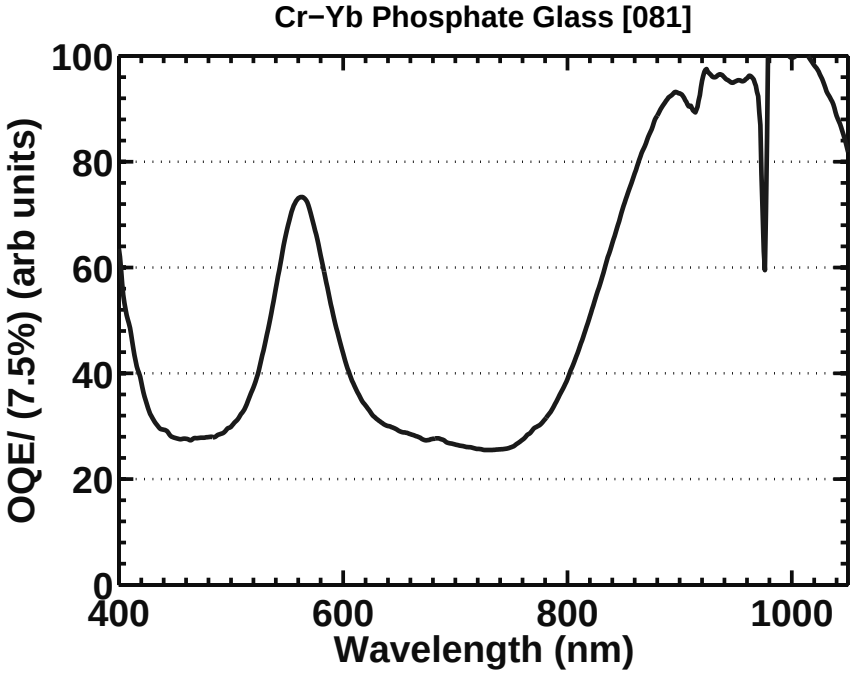

Figure 3-1: Efficiency of the first energy transfer event from Cr to Yb.

Chromium has a broadband absorption that extends into the near infrared. The absorption efficiency of a rare earth LSC would be greatly enhanced if sensitized with

Cr; however, Cr has an energy transfer complication. Back energy transfer from the rare earth activator to Cr reduces the photoluminescence efficiency so greatly that sensitization with Cr actually reduces overall device performance. Single handedly, this factor rules out Cr as a possible sensitization agent for rare earth LSCs.

3.2 Ti(III) Oxide

Titanium (III) oxide with an electronic structure of $3d^1$ exhibits ligand field broadened transitions between its 3d orbitals. Octahedrally coordination by oxygen atoms with a slight tetragonal distortion [19] is the source of the two overlapping absorption bands that peak at 580 and 700 nm, Figure 2-6. Attempts to obtain photoluminescence from the Ti (III) samples were unsuccessful and no forward energy transfer was demonstrated for this system, which contrasts previous literature.

3.2.1 Literature Review: Ti (III) sensitization of Rare Earth Elements

Two different research groups and one additional publication have reported the luminescent properties of Ti (III) in a phosphate glass matrix [14, 15, 20]. Others have reported on the location of peak absorption and ligand field strength within various oxide glasses [19, 21, 22]. The most extensive work was carried out by a group in Russia who worked on Ti (III) sensitized glasses in the late 1990's and early 2000's, and gave rise to more than 15 published papers demonstrating Ti (III) absorption, luminescence, or energy transfer to a rare earth ion. One publication explicitly indicated that back energy transfer from Nd or Yb to Ti (III) was not observed and stated that the $3d^1$ electronic structure of Ti (III) prevented back energy transfer [23]. The reported absence of back energy transfer and broadband absorption covering the visible and near infrared makes Ti (III) an excellent potential sensitizer for

LSC applications. Although our observed absorption coefficient for Ti (III) agrees with literature, we were unable to duplicate the photoluminescence or forward energy transfer previously reported for Ti (III).

3.2.2 Discussion of Ti (III) Absorption

For titanium the preferred oxidation state at standard temperature and pressure is Ti (IV), not Ti (III). Melting the glass in a reducing environment promotes Ti (III) formation over Ti (IV). Batyeav and Leonov describe previous techniques utilized to obtain Ti (III) [24] and found that hydrogen gas mixtures were the most effective means of reducing Ti (IV) to Ti(III). Our glass melting furnace was constructed with a gas mixing system designed to flow various reducing gas mixtures, including hydrogen gas mixtures. We empirically determined most useful composition of 5% H_2-95% N_2 which provides a reducing atmosphere that yields almost a complete reduction of Ti (IV) to Ti (III), determined through measuring the absorption coefficient for various H_2-N_2 mixtures, without affecting the mechanical properties of the glass. To confirm the presence of Ti (III) we referenced, Figure 3-2 from Batyaev and Leonov [15] which shows the molar absorption coefficient for Ti (III). The molar absorption coefficient is reportedly changing for different concentrations of Ti; a possible explanation is incomplete conversion of Ti (IV) to Ti (III). If for different concentrations of Ti there exists differing ratios between the concentrations of Ti (III) and Ti (IV), the apparent molar absorption coefficient would change. The values for the molar absorption coefficient in Figure 3-2 are drastically different from Figure 2-6. However, this thesis defines the absorption coefficient, and in turn, the molar absorption coefficient, using log base e rather than base 10, which was commonly used in the late 1990's. Figure 3-3 is the measured molar absorption coefficient for Ti replotted in log base 10; the measured values are now in line with those in Figure 3-2. Figure 2-6 is a representative absorption spectra of more than 50 samples that were synthesized in

our attempts to obtain PL or energy transfer from Ti(III). Our sample compositions span the majority of the glass forming regions of the P_2O_5-Al_2O_3-K_2O system.

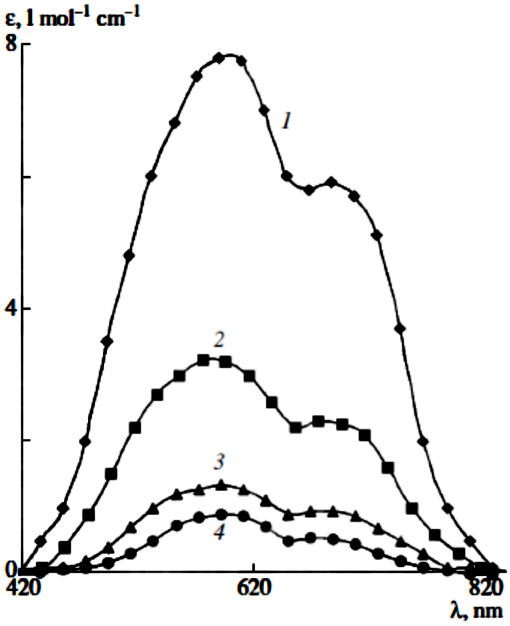

Fig. 1. Absorption spectra of PAPGs activated by trivalent titanium ions with different concentrations: (*1*) 0.1, (*2*) 0.2, (*3*) 0.25, and (*4*) 0.36 mol/l. The measurement temperature is 293 K.

Figure 3-2: Figure from Batyaev and Leonov, including the caption, of the molar absorption coefficient for Ti (III) in a phosphate glass and for various Ti concentrations.

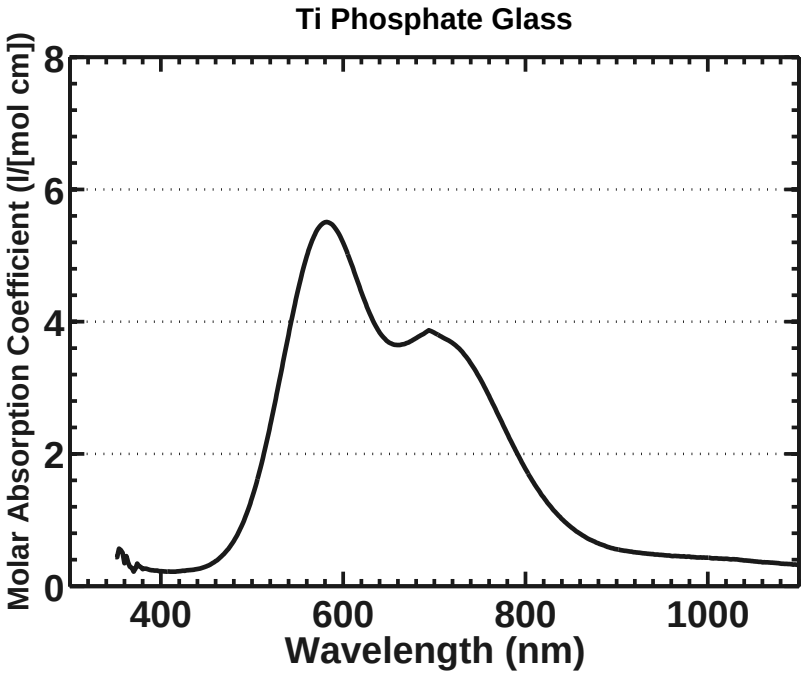

Figure 3-3: Molar absorption coefficient measured in this work replotted with a log base 10 molar absorption coefficient.

Even with absorption spectra matching previously reported values for Ti (III) glass, photoluminescence was not observed from any Ti (III) samples. This leads to the conclusion that the photoluminescence efficiency of Ti (III) is near zero; thus, it is not a suitable material for use in sensitized LSCs.

3.3 Vanadium (IV) Oxide

V (IV) oxide is isovalent with Ti (III) and also exhibits broadened transitions between its 3d orbitals due to ligand field splitting. The oxygen V (IV) coordination was characterized as tetragonally distorted octahedral by Ballhausen [25]. The strong tetrahedral distortion creates three absorption bands that peak at 452, 700, and 830 nanometers as shown in Figure 2-7. Photoluminescence from the V (IV) was observed, and successful forward energy transfer has been demonstrated.

3.3.1 Literature Review: V (IV) Absorption and Emission

The absorption spectra of V (IV) reported here is similar to previously documented work[16, 26], with the exception that previous work did not observe as distinct of a third absorption band in the blue. The third absorption band with a peak at 460 nm is likely more distinct due to the particular ligand field strength of our phosphate glass matrix. The only prior report of V (IV) photoluminescence is from Batyaev et al. [16] and is featured in Figure 3-4. Photoluminescence in Figure 2-14 closely matches that reported in this work.

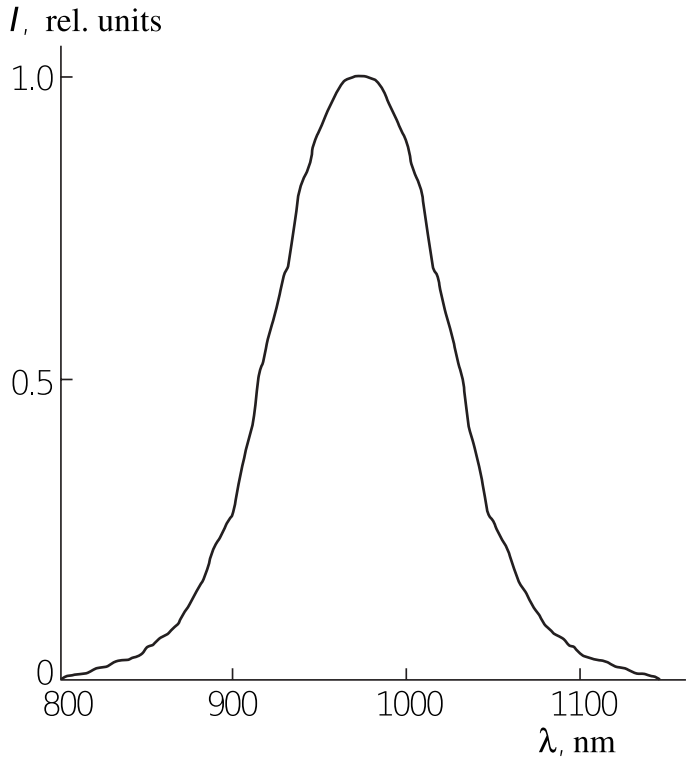

Fig. 2. Luminescence spectrum of potassium aluminophosphate glass doped with four-valence vanadium.

Figure 3-4: Photoluminescence of four valent V from Batyaev et al. including the figure caption.

3.3.2 Discussion of Observed Energy Transfer

To the author's knowledge, this work contains the first report of V (IV) to rare earth ion energy transfer in a phosphate glass. The absence of V (IV) emission in the photoluminescence spectrum of co-doped glasses is a possible indicator that back energy transfer is not occurring. Further investigations of the energy transfer characteristics are ongoing.

3.4 Conclusion and Future Work

Chromium (III), titanium (III), and vanadium (IV) sensitization of Yb (III) and Nd (III) for LSC applications has been studied. It was found that back energy transfer from the rare earth ion to Cr (III) lowers the photoluminescence quantum yield of Cr (III) sensitized samples, thus eliminating it as a candidate for use in sensitized LSCs. Ti (III) was also found to have a zero photoluminescence quantum yield, which eliminates it, too, as a reasonable material for sensitizing LSCs. V (IV) has been found to energy transfer to both Nd (III) and Yb (III) with preliminary indications from photoluminescence measurements that the back energy transfer process may be reduced due to the $3d^1$ electronic structure.

Preliminary experiments to determine if back energy transfer occurs in the V-Nd co-doped system are ongoing and suggest that it does not. Future work will confirm these experiments and extend the results to a V (IV) and Yb (III) system. Optimization of the V (IV) PLQE and fabrication of a working LSC based on V (IV) will occur subsequent to these experiments.

Appendix A

Tables

Table A.1: XPS compositions for samples measured by XPS.

Sample	P_2O_5	Al_2O_3	K_2O
3	40.78	16.12	43.10
38	57.72	27.09	15.20
39	58.46	15.67	25.87
43	43.42	26.10	30.48
52	61.24	22.26	16.50
69	64.28	31.03	4.68
70	49.08	27.98	22.94
82	56.61	38.27	5.12
83	59.86	10.28	29.86
84	58.73	12.73	28.54
95	61.47	9.29	29.24
96	59.68	8.97	28.24
101	59.10	6.11	24.07
102	59.81	4.34	25.41
103	58.93	14.96	21.55
104	60.93	5.91	23.61
108	60.68	9.68	19.70

Reported molar percentrages of P_2O_5- Al_2O_3 - K_2O are determined from the relative elemental percentages using XPS. Sample 065 was batched and processed identically to sample 069, it is assumed that the composition of the samples is identical.

Bibliography

[1] D. L. Dexter, "A theory of sensitized luminescence in solids," *The Journal of Chemical Physics*, vol. 21, no. 5, p. 836, 1953.

[2] T. Forster, "Transfer mechanisms of electronic excitation energy," *Radiation Research Supplement*, vol. 2, pp. 326–339, Jan. 1960. ArticleType: research-article / Issue Title: Bioenergetics: Considerations of Processes of Absorption, Stabilization, Transfer, and Utilization. Proceedings of a Symposium Sponsored by the U. S. Atomic Energy Commission Held at Brookhaven National Laboratory, October 12-16, 1959 / Full publication date: 1960 / Copyright 1960 Radiation Research Society.

[3] W. H. Weber and J. Lambe, "Luminescent greenhouse collector for solar radiation," *Applied Optics*, vol. 15, pp. 2299–2300, Oct. 1976.

[4] M. J. Currie, J. K. Mapel, T. D. Heidel, S. Goffri, and M. A. Baldo, "High-Efficiency organic solar concentrators for photovoltaics," *Science*, vol. 321, pp. 226 –228, July 2008.

[5] B. Rowan, L. Wilson, and B. Richards, "Advanced material concepts for luminescent solar concentrators," *Selected Topics in Quantum Electronics, IEEE Journal of*, vol. 14, no. 5, pp. 1312–1322, 2008.

[6] J. S. Batchelder, A. H. Zewail, and T. Cole, "Luminescent solar concentrators. 2: Experimental and theoretical analysis of their possible efficiencies," *Applied Optics*, vol. 20, pp. 3733–3754, Nov. 1981.

[7] J. S. Batchelder, A. H. Zewail, and T. Cole, "Luminescent solar concentrators. 1: Theory of operation and techniques for performance evaluation," *Applied Optics*, vol. 18, no. 18, pp. 3090–3110, 1979.

[8] R. K. Brow, "Nature of alumina in phosphate glass: I, properties of sodium aluminophosphate glass," *Journal of the American Ceramic Society*, vol. 76, pp. 913–918, Apr. 1993.

[9] R. Reisfeld and C. K. Jrgensen, "Luminescent solar concentrators for energy conversion," in *Solar Energy Materials*, vol. 49, pp. 1–36, Berlin, Heidelberg: Springer Berlin Heidelberg, 1982.

[10] R. Reisfeld and A. Kisilev, "Concentration dependence of energy transfer between chromium (III) and neodymium (III) in lithium-lanthanum-phosphate glasses," *Chemical Physics Letters*, vol. 115, pp. 457–462, Apr. 1985.

[11] B. Jezowska-Trzebiatowska, E. Lukowiak, W. S. cedilla]k, A. Buczkowski, S. Patela, J. Radojewski, and J. Sarzynski, "Neodymium-chromium doped phosphate glasses as luminescent solar concentrators," *Solar Energy Materials*, vol. 13, pp. 267–277, May 1986.

[12] L. J. Andrews, B. C. McCollum, and A. Lempicki, "Luminescent solar collectors based on fluorescent glasses," *Journal of Luminescence*, vol. 24-25, pp. 877–880, Nov. 1981.

[13] N. Neuroth and R. Haspel, "Glasses for luminescent solar concentrators," *Solar Energy Materials*, vol. 16, pp. 235–242, Aug. 1987.

[14] L. E. Bausa, F. Jaque, J. G. Sole, R. Cases, and A. Duran, "Photoluminescence of ti3+ in phosphate glasses," *Journal of Luminescence*, vol. 40-41, pp. 193–194, Feb. 1988.

[15] I. M. Batyaev and A. V. Leonov, "Optical properties of potassium aluminum phosphate glass activated by trivalent titanium ions," *Optics and Spectroscopy*, vol. 99, no. 4, p. 584, 2005.

[16] I. M. Batyaev, S. V. Linnikov, and A. L. Lipatova, "Spectral luminescence properties of potassium aluminophosphate glass doped with four-valence vanadium complexes," *Optics and Spectroscopy*, vol. 96, no. 6, pp. 850–852, 2004.

[17] S. Mizuno, H. Ito, K. Hasegawa, H. Nasu, M. Hughes, T. Suzuki, and Y. Ohishi, "The efficiencies of energy transfer from cr to nd ions in silicate glasses," (San Francisco, California, USA), pp. 75980A–75980A–8, 2010.

[18] R. Reisfeld, "Future technological applications of rare-earth-doped materials," *Journal of the Less Common Metals*, vol. 93, pp. 243–251, Sept. 1983.

[19] A. Paul, "Optical and esr spectra of titanium (III) in Na2O-B2O3 and Na2O-P2O5 glasses," *Journal of Materials Science*, vol. 10, pp. 692–696, Apr. 1975.

[20] H. Eilers, U. Hmmerich, S. Jaffe, and W. Yen, "Refractive index changes in ti3+-doped glass," *Optics Communications*, vol. 101, pp. 188–191, Aug. 1993.

[21] K. Moringa, H. Yoshida, and H. Takebe, "Compositional dependence of absorption spectra of ti3+ in silicate, borate, and phosphate glasses," *Journal of the American Ceramic Society*, vol. 77, pp. 3113–3118, Dec. 1994.

[22] D. A. Nolet, "Optical absorption and mssbauer spectra of fe, ti silicate glasses," *Journal of Non-Crystalline Solids*, vol. 37, pp. 99–110, Mar. 1980.

[23] I. M. Batyaev and E. B. Kleshchinov, "Sensitization of ytterbium luminescence by trivalent titanium ions in aluminosilicate phosphate glass," *Technical Physics Letters*, vol. 22, pp. 494–495, June 1996.

[24] I. M. Batyaev and A. V. Leonov, "Technological aspects of melting of potassium aluminophosphate glasses activated with trivalent titanium," *Glass Physics and Chemistry*, vol. 30, pp. 425–427, Sept. 2004.

[25] C. J. Ballhausen and H. B. Gray, "The electronic structure of the vanadyl ion," *Inorganic Chemistry*, vol. 1, pp. 111–122, Feb. 1962.

[26] R. V. S. S. N. Ravikumar, V. R. Reddy, A. V. Chandrasekhar, B. J. Reddy, Y. P. Reddy, and P. S. Rao, "Tetragonal site of transition metal ions doped sodium phosphate glasses," *Journal of Alloys and Compounds*, vol. 337, pp. 272–276, May 2002.